frontiers | Frontiers in Molecular Biosciences

TYPE Original Research
PUBLISHED 12 February 2024
DOI 10.3389/fmolb.2024.1328077

OPEN ACCESS

EDITED BY
Zhen-Yu She,
Fujian Medical University, China

REVIEWED BY
Peng Dong,
Chinese Academy of Sciences (CAS), China
Cheuk Tung Leung,
University of Minnesota Twin Cities, United States

*CORRESPONDENCE
Jason Stumpff,
jstumpff@uvm.edu

†These authors have contributed equally to this work

RECEIVED 26 October 2023
ACCEPTED 08 January 2024
PUBLISHED 12 February 2024

CITATION
Schutt KL, Queen KA, Fisher K, Budington O, Mao W, Liu W, Gu X, Xiao Y, Aswad F, Joseph J and Stumpff J (2024), Identification of the KIF18A alpha-4 helix as a therapeutic target for chromosomally unstable tumor cells.
Front. Mol. Biosci. 11:1328077.
doi: 10.3389/fmolb.2024.1328077

Identification of the KIF18A alpha-4 helix as a therapeutic target for chromosomally unstable tumor cells

Katherine L. Schutt[1†], Katelyn A. Queen[1†], Kira Fisher[1], Olivia Budington[1], Weifeng Mao[2], Wei Liu[2], Xiaohui Gu[2], Yisong Xiao[2], Fred Aswad[3], James Joseph[3] and Jason Stumpff[1*]

[1]Department of Molecular Physiology and Biophysics, University of Vermont, Burlington, VT, United States, [2]Apeiron Therapeutics, Shanghai, China, [3]Apeiron Therapeutics, Burlingame, CA, United States

Background: The mitotic kinesin, KIF18A, is required for proliferation of cancer cells that exhibit chromosome instability (CIN), implicating it as a promising target for treatment of a subset of aggressive tumor types. Determining regions of the KIF18A protein to target for inhibition will be important for the design and optimization of effective small molecule inhibitors.

Methods: In this study, we used cultured cell models to investigate the effects of mutating S284 within the alpha-4 helix of KIF18A, which was previously identified as a phosphorylated residue.

Results: Mutations in S284 cause relocalization of KIF18A from the plus-ends of spindle microtubules to the spindle poles. Furthermore, KIF18A S284 mutants display loss of KIF18A function and fail to support proliferation in CIN tumor cells. Interestingly, similar effects on KIF18A localization and function were seen after treatment of CIN cells with KIF18A inhibitory compounds that are predicted to interact with residues within the alpha-4 helix.

Conclusion: These data implicate the KIF18A alpha-4 helix as an effective target for inhibition and demonstrate that small molecules targeting KIF18A selectively limit CIN tumor cell proliferation and result in phenotypically similar effects on mitosis at the single cell level compared to genetic perturbations.

KEYWORDS

mitosis, kinesin, spindle, KIF18A, chromosome instability, small-molecule inhibitor

Introduction

Faithful replication and segregation of chromosomes are essential for maintaining genomic integrity. Chromosomal instability (CIN) is a hallmark of tumor cells, where cells exhibit frequent gain or loss of whole chromosomes (Lengauer et al., 1998). These frequent missegregration events are, in part, due to inherent differences in CIN cells, such as increased microtubule plus-end assembly rates, aberrant kinetochore–microtubule attachments, and defects in the spindle assembly checkpoint (SAC) (Thompson et al., 2010; Gordon et al., 2012; Ertych et al., 2014). Although CIN can lead to increased tumorigenesis and therapeutic resistance (Bach et al., 2019), recent efforts have focused on methods for targeting CIN as a possible Achilles' heel to selectively target and eliminate

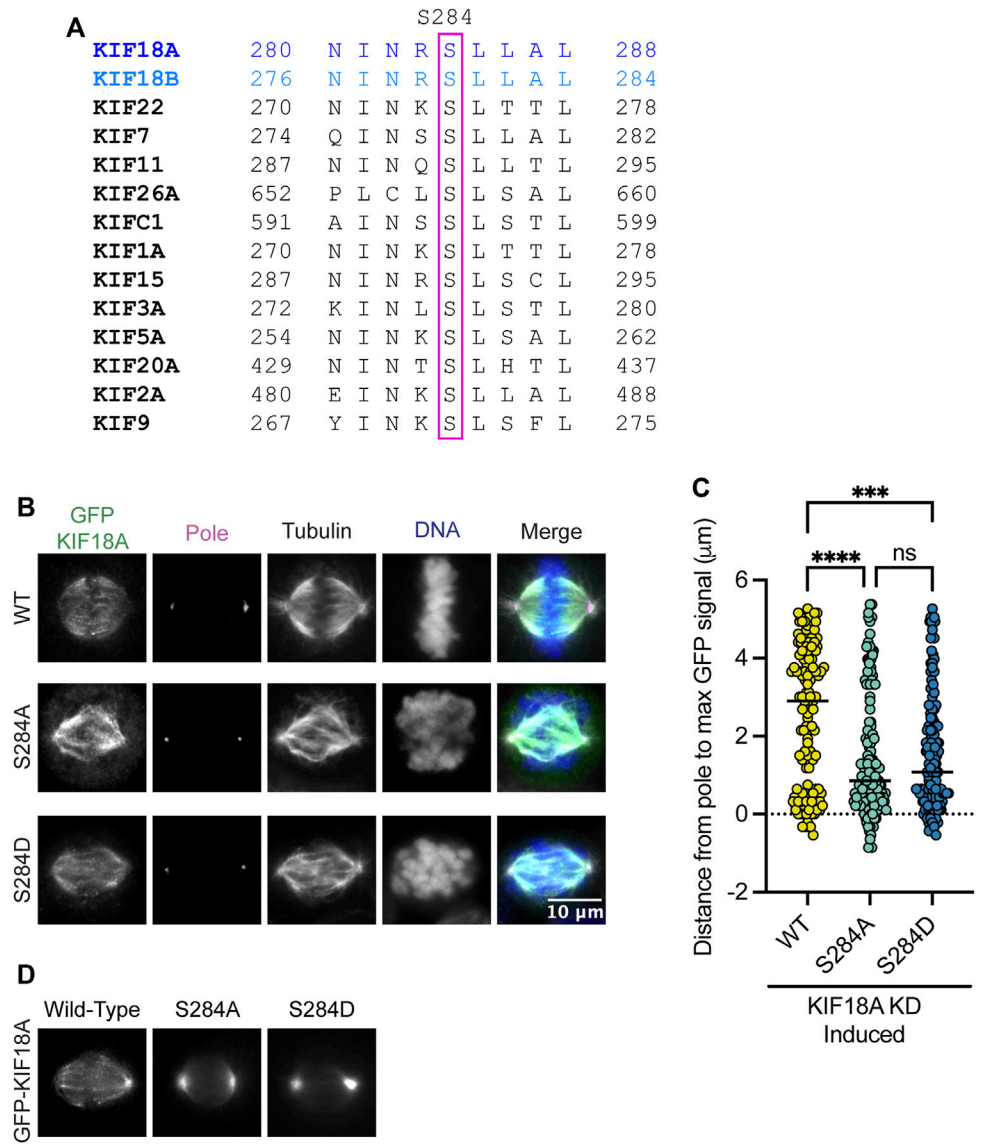

FIGURE 1
Mutation of KIF18A S284 alters its localization. **(A)** Sequence alignment of the alpha-4 region from kinesin family proteins. **(B)** Immunofluorescence images of HeLa Kyoto GFP-KIF18A inducible cells fixed and stained 24 h after endogenous KIF18A knockdown and induction of the indicated GFP-KIF18A construct. Scale bar = 2 µm. Text colors indicate pseudo color in a merged image. From left to right, KIF18A antibody staining, γ-tubulin antibody staining, α-tubulin antibody staining, DNA/DAPI, and merged image. **(C)** Quantification of the distance from the pole to the maximum GFP-KIF18A signal in HeLa Kyoto cells using line scan analysis. Fluorescence values were normalized and aligned to the peak pole (γ-tubulin) signal intensity. The solid line indicates the median. Each dot represents an individual line scan. HeLa Kyoto GFP-KIF18A WT = 136 line scans, GFP-S284D = 130 line scans, and GFP-S284A = 144 line scans. Data acquired from three experimental replicates. Statistical results shown for a Kruskal–Wallis with Dunn's multiple comparisons test; *p* values: <0.05 (*), <0.01 (**), <0.001 (***), and <0.0001 (****). n.s. indicates not significant (>0.05). **(D)** Representative images of the indicated GFP-KIF18A constructs in live cells.

tumor cells. Common therapeutic strategies for treatment of tumors directly target the altered microtubule dynamics of CIN cells with microtubule-targeting agents (MTAs) such as paclitaxel, which stabilizes microtubules and induces mitotic arrest or aberrant chromosome segregation (Jordan and Wilson, 2004; Weaver, 2014). Although many MTAs have shown promising results in preclinical studies, clinical application of MTAs in patients has caused off-target effects and cytotoxicity, necessitating additional therapeutic options (Zasadil et al., 2014; Tischer and Gergely, 2018).

Selectively targeting CIN requires identifying the genetic dependency of chromosomally unstable cells versus diploid cells. Several recent studies revealed the specific dependency of CIN cells, but not diploid cells, on the kinesin-8 KIF18A (Cohen-Sharir et al., 2021; Marquis et al., 2021; Quinton et al., 2021). KIF18A accumulates at the plus-ends of microtubules, where it suppresses microtubule dynamics to promote chromosome alignment during the metaphase (Mayr et al., 2007; Stumpff et al., 2008; du et al., 2010). Loss of KIF18A in multiple cell lines with CIN leads to decreased proliferation, multipolar spindles, and cell death (Cohen-Sharir et al., 2021; Marquis et al., 2021; Quinton et al., 2021). Importantly, these effects were not observed upon KIF18A knockdown (KD) in diploid

cell lines (Cohen-Sharir et al., 2021; Marquis et al., 2021; Quinton et al., 2021). These results suggest that KIF18A is a promising therapeutic target for CIN cells.

Identifying the molecular regions of KIF18A for targeting via small-molecule inhibitors will be an important step in pursuing KIF18A inhibition as a therapeutic strategy. KIF18A activity is normally regulated during mitosis via binding to kinesin family-binding protein (KIFBP) (Malaby et al., 2019). KIFBP inhibits the activities of KIF18A and of a subset of other kinesins by altering the conformation of the conserved alpha-4 helix within the motor domain, which in turn reduces the interaction of kinesins with the microtubules (Atherton et al., 2020; Solon et al., 2021). A novel series of KIF18A inhibitors, which are currently being tested in clinical trials, have also been predicted to contact the alpha-4 helix region of KIF18A (Tamayo et al., 2022). Thus, the alpha-4 helix may represent an important site for regulating KIF18A activity. Consistent with this, a serine residue within the alpha-4 helix (S284) has been identified as a phospho-residue via mass spectrometry (Mertins et al., 2014). Here, we demonstrate that modulation of KIF18A activity through S284 mutations or chemical inhibition causes similar relocalization of the protein within the spindle and reduces proliferation of CIN cells. These results confirm that multiple CIN tumor types depend on KIF18A activity and provide support for targeting KIF18A's alpha-4 helix region, which is a treatment strategy for chromosomally unstable tumors.

Results

Alteration at serine 284 in the highly conserved alpha-4 helix results in accumulation of KIF18A at spindle poles

The alpha-4 helix in the motor domain of KIF18A is highly conserved across various kinesin families and KIF18A homologs (Figure 1A). The helix is known to play a role in microtubule binding and nucleotide gating (Hirokawa et al., 2009), facilitating the ability of the motor protein to move toward the plus-ends of microtubules. Mass spectrometry data indicate that serine 284 (S284) within the alpha-4 helix is phosphorylated in cells, suggesting that KIF18A activity may be regulated via alpha-4 helix phosphorylation (Mertins et al., 2014). To investigate the effects of charge changes at S284, we generated HeLa Kyoto cell lines that inducibly express GFP-tagged wild-type KIF18A, phospho-null KIF18A (S284A), or phosphomimetic KIF18A (S284D). Each construct contained siRNA-resistant, silent mutations, and the expression was induced following treatment with either control or KIF18A-specific siRNAs. Quantification of KIF18A immunofluorescence indicates that wild-type and mutant KIF18A constructs were expressed at similar levels (Supplementary Figure S1). Analysis of KIF18A localization revealed that both S284A and S284D KIF18A mutants result in accumulation of KIF18A protein near spindle poles rather than at kinetochore microtubule plus-ends (Figures 1B, C). This altered localization is unique compared to that of other reported KIF18A mutants that are predicted to compromise microtubule binding, suggesting that mutation of S284 may alter KIF18A activity through a mechanism that does not inhibit the interaction with microtubules (Stumpff et al., 2008; Kim et al., 2014; Czechanski et al., 2015). The pole localization was even more apparent in live cells expressing GFP-KIF18A constructs, where the S284D mutant had a more pronounced effect, with less evidence of motor accumulation on the mitotic spindle compared to the S284A mutant (Figure 1D).

Mutation of S284 leads to loss of KIF18A function

KIF18A KD leads to unaligned chromosomes and increased spindle length (Mayr et al., 2007; Stumpff et al., 2008). To investigate if mutations at S284 compromise KIF18A function during mitosis, we treated cells with siRNAs targeting KIF18A and induced the expression of wild-type, S284A, or S284D KIF18A-containing silent mutations that confer siRNA resistance. KIF18A function was assessed by measuring chromosome alignment and spindle length in late prometaphase and metaphase cells. We determined the full width at half maximum of the chromosome distribution within an individual cell as a metric of chromosome alignment (Stumpff et al., 2012; Fonseca and Stumpff, 2016). Wild-type KIF18A restored chromosome distribution to levels seen in control KD cells; however, the S284A and S284D mutants were unable to promote chromosome alignment (Figures 2A, B). Additionally, while wild-type KIF18A expression resulted in spindle lengths comparable to those in control cells, neither S284A nor S284D mutants were able to properly regulate spindle length (Figure 2C). This work indicates that mutation of S284 in alpha-4 helix results in loss of KIF18A function.

KIF18A S284D causes mitotic arrest and multipolar mitotic spindles

Chromosomally unstable cell lines depend on KIF18A for mitotic progression and maintenance of bipolar mitotic spindles (Cohen-Sharir et al., 2021; Marquis et al., 2021; Quinton et al., 2021). To determine if KIF18A S284 mutants are able to promote normal mitotic progression, we determined the percentage of HeLa cells in mitosis following KIF18A KD and expression of S284 mutants. While KIF18A-S284A was able to promote mitotic progression to a greater extent than KIF18A-S284D, both mutants resulted in a significant increase in the percentage of mitotic cells compared to controls (Figures 3A, B). These data indicate that cells expressing KIF18A-S284D experience delays in mitotic progression, similar to those occurring following KIF18A depletion (Mayr et al., 2007; Stumpff et al., 2008; Fonseca et al., 2019).

Loss of KIF18A function in chromosomally unstable cells also results in an increase in the number of mitotic cells with multipolar spindles (Marquis et al., 2021). To determine if S284 mutants can promote spindle bipolarity, the percentage of multipolar mitotic cells was determined following KIF18A KD and expression of wild-type or S284 mutant KIF18A. While wild-type and S284A KIF18A

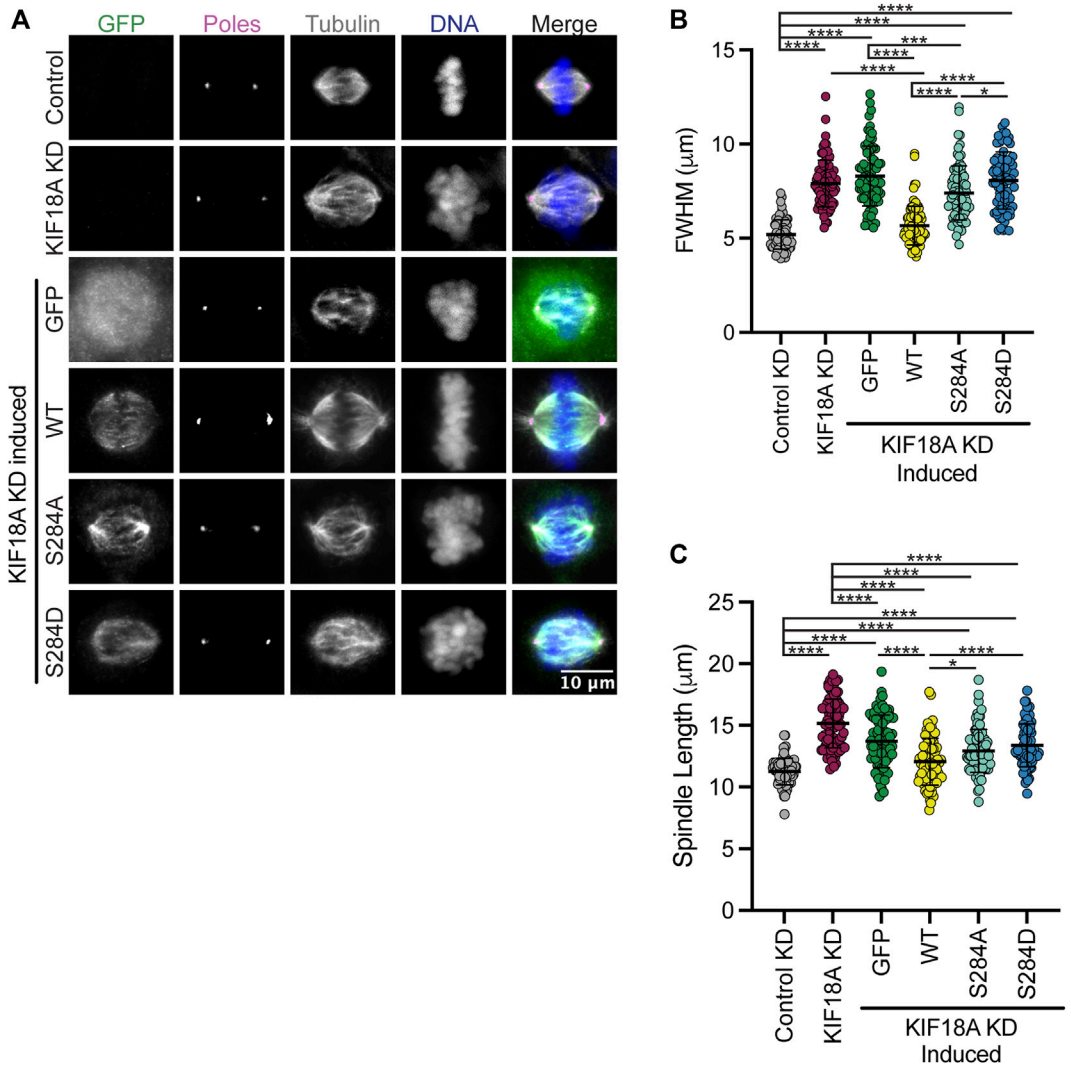

FIGURE 2
Expression of KIF18A S284 does not rescue KIF18A knockdown phenotypes. **(A)** Immunofluorescence images of HeLa Kyoto GFP KIF18A inducible cells fixed and stained 24 h after endogenous KIF18A knockdown and induction of the GFP KIF18A construct. Scale bar: 10 µm. Colors indicate pseudo color in a merged image. From left to right, GFP antibody staining, poles/γ-tubulin antibody staining, α-tubulin antibody staining, DNA/DAPI, and merged image. **(B)** Plot of full-width at half maximum values measured for chromosome distributions in HeLa Kyoto GFP KIF18A inducible cells. The solid horizontal line indicates mean, and vertical lines indicate standard deviation. Each dot represents a single cell. Data acquired from three experimental replicates. One-way ANOVA with Tukey's test for multiple comparisons was run, *p*-value: <0.05 (*), <0.01 (**), <0.001 (***), and <0.0001 (****). If no significance is indicated, differences were not significant (>0.05). **(C)** Quantification of spindle length in HeLa Kyoto GFP KIF18A inducible cells. The solid horizontal line indicates mean, and vertical lines indicate standard deviation. Each dot represents a single cell. The following cell numbers were analyzed for each condition in **(B,C)** control siRNA = 75, KIF18A siRNA = 84, GFP = 80, GFP-KIF18A WT = 81, GFP-S284A = 83, and GFP-S284D = 78. Data acquired from three experimental replicates. One-way ANOVA with Tukey's test for multiple comparisons was run. *p*-value style: <0.05 (*), <0.01 (**), <0.001 (***), and <0.0001 (****). If no significance is indicated, the result was not significant (>0.05).

expressing cells formed multipolar spindles at a level similar to those of controls, KIF18A-S284D expressing cells displayed a significant increase in multipolar spindles, which are similar to levels seen following KIF18A KD alone (Figures 3C, D).

KIF18A-S284D expressing cells display reduced proliferation

Mitotic arrest and multipolar spindles in KIF18A-depleted, chromosomally unstable tumor cells strongly correlate with decreased proliferation (Marquis et al., 2021). To probe if the expression of KIF18A-S284 mutants also results in proliferation defects, we performed a microscopy-based kinetic proliferation assay in cells treated with KIF18A siRNAs expressing wild-type or S284 mutant KIF18A (Marquis et al., 2021). Cell populations expressing GFP alone or KIF18A-S284D displayed significantly lower proliferation during a 5-day time-course than cells expressing wild-type or KIF18A-S284A (Figures 4A–C). The observed decrease in proliferation for KIF18A-S284D correlates with the measured effects of this mutant on mitotic arrest and spindle multipolarity.

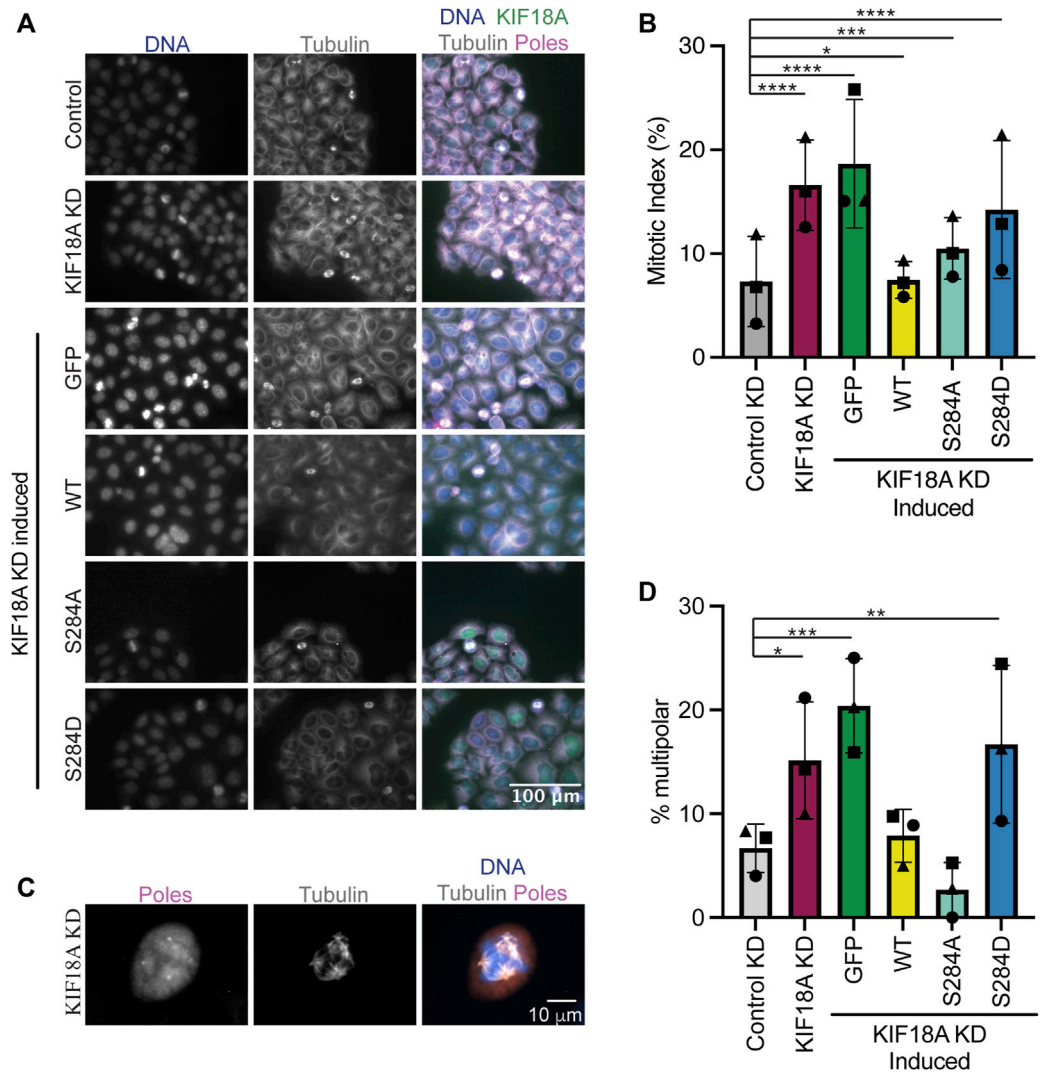

FIGURE 3
Mutation of KIF18A S284 to S284D leads to mitotic arrest and multipolar spindles. **(A)** Immunofluorescence images of HeLa Kyoto GFP KIF18A inducible cells fixed and stained 24 h after endogenous KIF18A knockdown and induction of the GFP KIF18A construct. Scale bar: 100 µm. Colors indicate pseudo color in a merged image. From left to right, DNA/DAPI, α-tubulin antibody staining, and merged image. The merged image includes KIF18A and spindle pole antibody staining in addition to DNA and α-tubulin antibody staining. **(B)** Quantification of the mitotic index (% cells in mitosis) in HeLa Kyoto GFP KIF18A inducible cell lines. **(C)** Representative image of a multipolar spindle in a KIF18A KD cell. **(D)** Quantification of multipolarity (% multipolar cells) in HeLa Kyoto GFP KIF18A inducible cell lines. Bars in **(B,D)** indicate overall mean, the circles indicate mean from experimental replicate 1, the squares indicate mean from experimental replicate 2, and the triangles indicate the mean from experimental replicate 3. Total number of cells analyzed for HeLa Kyoto: KIF18A KD = 1402, GFP = 997, GFP-KIF18A WT = 2136, GFP-S284A = 1364, and GFP-S284D = 1574. Data were compared using a chi-squared test. *p*-value style: <0.05 (*), <0.01 (**), <0.001 (***), and <0.0001 (****). If no significance is indicated, the result was not significant (>0.05).

Chemical inhibition of KIF18A with Compound 3 or Sovilnesib phenocopies KIF18A knockdown phenotypes

Interestingly, S284 in KIF18A is located adjacent to residues within the alpha-4 helix that are proposed to form a binding pocket for a series of recently described KIF18A inhibitors (Tamayo et al., 2022). One of these inhibitors, Sovilnesib, is currently being tested in clinical trials (Identifier: NCT04293094) for treating patients with advanced p53-mutated tumors, highlighting the therapeutic potential of KIF18A-targeting drugs. If these inhibitors inactivate KIF18A through effects on alpha-4, we might expect the specific phenotypes caused by the expression of KIF18A-S284 mutants and inhibitor treatment to be similar. To address this question, we synthesized Sovilnesib, as well as a similar derivative with a single-heteroatom substitution (Tamayo et al., 2022), hereafter referred to as Compound 3 (Figure 5A). Biochemical studies *in vitro* with purified KIF18A revealed a half-maximal inhibitory concentration (IC_{50}) of 8.2 nM (nM) for Compound 3 and 41.3 nM for Sovilnesib (Figure 5B). These results confirm that Compound 3 and Sovilnesib are potent inhibitors of KIF18A's microtubule-stimulated ATPase activity.

To determine whether these compounds inhibit KIF18A in cells, we treated chromosomally unstable triple-negative breast cancer (TNBC) MDA-MB-231 cells for 24 h with dimethyl sulfoxide (DMSO), 250 nM Compound 3 or Sovilnesib, control siRNA, or

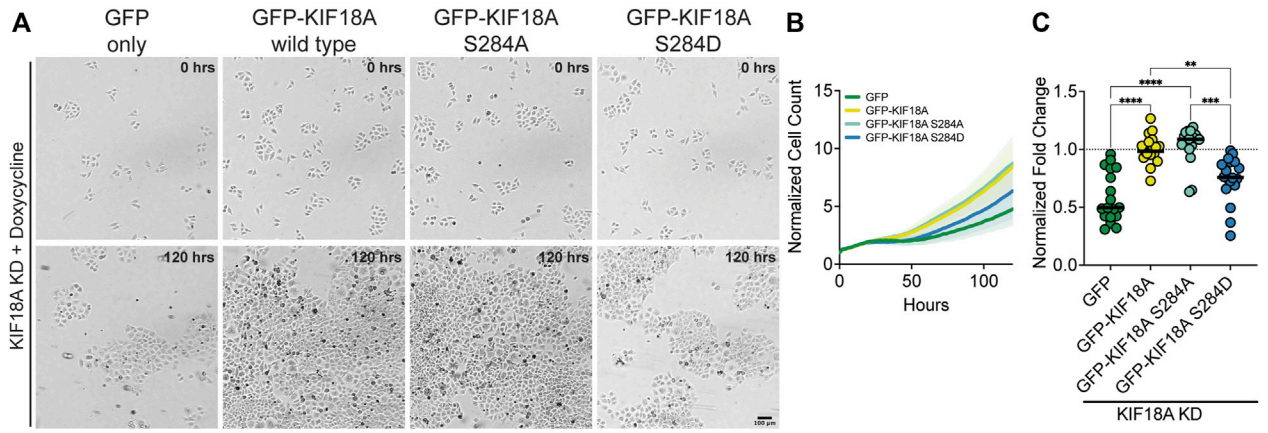

FIGURE 4
Phospho-mimetic mutation of KIF18A S284 leads to decreased proliferation of HeLa Kyoto cells. **(A)** Brightfield images of HeLa Kyoto cells from time-lapse proliferation assays after knockdown of endogenous KIF18A and induced expression of the indicated construct. Scale bar: 100 μm. (Top) 0 h and (bottom) 120 h. **(B)** Normalized cell count versus time (hours) from automated brightfield imaging. The cell counts from each timepoint were normalized to the number of cells at the initial timepoint. Lines represent means, and shaded areas represent standard deviation. Data shown from three experimental replicates. **(C)** Normalized fold-change after 120 h for each condition. All conditions were normalized to GFP-KIF18A wild-type rescue, indicated by the dotted line. Each dot represents an individual well of cells. Data shown from three experimental replicates. Statistical results are shown for a Kruskal–Wallis with Dunn's multiple comparisons test. *p*-value style: <0.05 (*), <0.01 (**), <0.001 (***), and <0.0001 (****). n.s. indicates not significant (>0.05).

KIF18A siRNA and measured the chromosome alignment and spindle length (Figures 5C–E; Supplementary Figure S2). Treatment of cells with KIF18A siRNA or 250 nM KIF18A inhibitor resulted in increased spindle length (Figure 5D; Supplementary Figure S2A) as compared to control siRNA and DMSO treatment. Similarly, treatment of MDA-MB-231 cells with 250 nM KIF18A inhibitor led to defects in chromosome alignment, though to a lesser extent when compared to treatment of MDA-MB-231 cells with KIF18A KD (Figure 5E; Supplementary Figure S2B). The difference in the magnitude of the shift in chromosome alignment between Compound 3 and KIF18A siRNA treatment may represent biological differences in inhibition versus KD due to the continued presence of the KIF18A protein. Together, these results suggest that chemical inhibition of KIF18A by Compound 3 mimics KIF18A siRNA KD phenotypes in MDA-MB-231 cells.

KIF18A accumulates at spindle poles following inhibitor treatment

One defining feature of the KIF18A-S284 mutants is their accumulation at spindle poles when expressed in mitotic cells (Figure 1B). Normally, KIF18A accumulates at the plus-ends of microtubules, where it regulates chromosome movements and promotes chromosome alignment during the metaphase (Mayr et al., 2007; Stumpff et al., 2008; Stumpff et al., 2012). To determine if KIF18A inhibitor treatment leads to similar aberrant KIF18A localization away from microtubule plus-ends, we measured KIF18A localization in multiple cell types after treatment with 250 nM Compound 3, Sovilnesib, or DMSO control. To confirm changes in KIF18A localization in both chromosomally stable and unstable cell lines, we used diploid retinal pigment epithelial-1 (RPE1) cells and two chromosomally unstable cell lines, colorectal adenocarcinoma HT-29 cells and MDA-MB-231 cells. In all cell types, we observed a shift in the localization of KIF18A away from microtubule plus-ends toward the spindle poles (Figures 6A–F; Supplementary Figure S3). To quantify this change in localization, line scan analyses were conducted to determine the distance from the spindle pole to the maximum KIF18A signal in each half-spindle. Cells treated with DMSO had characteristic accumulation of KIF18A toward the plus-ends of microtubules several microns away from the pole, whereas cells treated with 250 nM Compound 3 or Sovilnesib exhibited accumulation of KIF18A in the vicinity of the spindle poles (Figures 6A–F; Supplementary Figures S3A, S3B). These results demonstrate that KIF18A inhibitor treatment leads to dynamic accumulation of KIF18A at spindle poles in both chromosomally stable and unstable cell types.

KIF18A localization analyses in fixed-cell experiments showed accumulation of the motor at the spindle poles in KIF18A inhibitor-treated cells, similar to KIF18A-S284 mutants. To confirm these results in live cells and determine the kinetics of KIF18A relocalization from microtubule plus-ends to spindle poles, we generated an hTERT-RPE1 cell line that inducibly expresses GFP-tagged KIF18A (hereafter, RPE1 GFP-KIF18A). We arrested RPE1 GFP-KIF18A cells in the metaphase with MG-132 and then added DMSO or Compound 3 to track changes in KIF18A localization. In DMSO-treated cells, GFP-KIF18A remained at the plus-ends of microtubules throughout the course of imaging (Figure 7A). In contrast, we observed loss of KIF18A from the plus-ends of microtubules and accumulation of KIF18A at spindle poles within minutes of Compound 3 addition (Figure 7A). This relocalization occurred in a pattern where a gap in KIF18A protein localization at the center of the spindle was observed a few minutes after compound addition, and the gap then expanded toward the poles over time. We quantified these changes in KIF18A localization by plotting the GFP-KIF18A fluorescence profile across the spindle in the "Initial" timepoint (pre-DMSO or Compound

10.3389/fmolb.2024.1328077

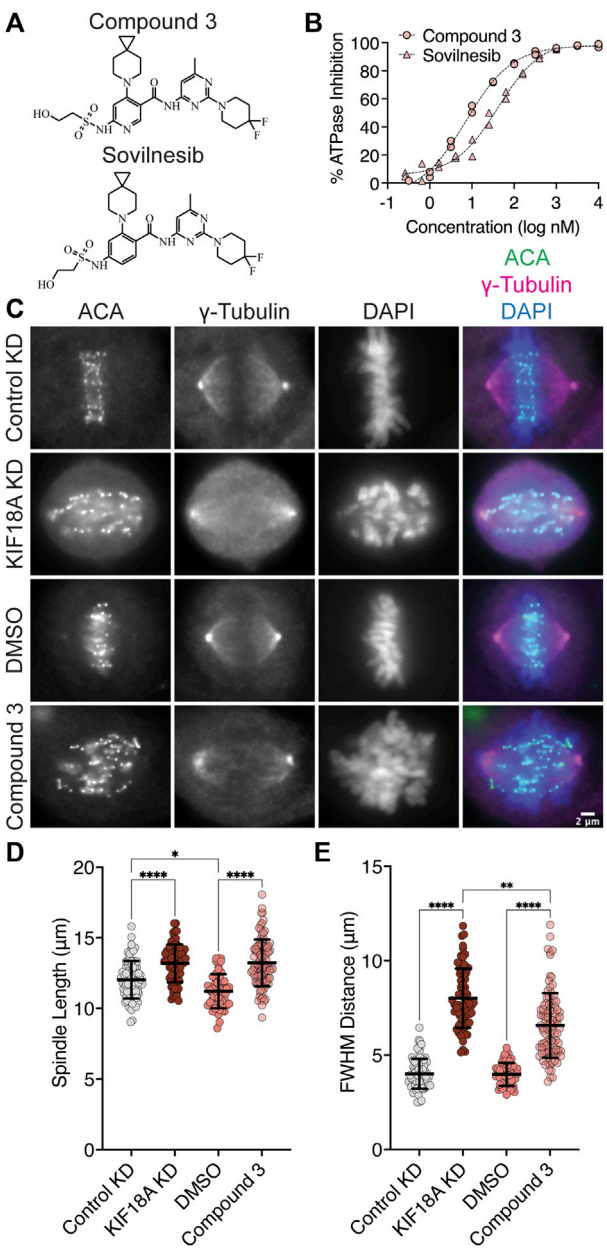

FIGURE 5
KIF18A inhibitors mimic KIF18A knockdown phenotypes in MDA-MB-231 cells. **(A)** Chemical structure of Compound 3. **(B)** % inhibition of KIF18A microtubule stimulated ATPase activity *in vitro* versus logarithmic concentration of the indicated KIF18A inhibitors. Representative data from two experimental replicates of each is shown. Dashed lines indicate non-linear fit of the data. **(C)** Immunofluorescence images of MDA-MB-231 cells fixed and stained after 24 h of indicated treatments. Scale bar: 2 µm. **(D)** Graph of spindle lengths measured in cells fixed and stained 24 h after the indicated treatments. **(E)** Graph of full-width at half maximum of centromere fluorescence distribution along the length of the spindle measured in cells fixed and stained 24 h after the indicated treatments. For **(D–E)**, each dot represents a single cell. Mean ± standard deviation is displayed. Statistical results are shown for a Kruskal–Wallis with Dunn's multiple comparisons test. *p*-value style: <0.05 (*), <0.01 (**), <0.001 (***), and <0.0001 (****). n.s. indicates not significant (>0.05). The following cell numbers were analyzed: Control siRNA = 76, KIF18A siRNA = 69, DMSO = 51, and Compound 3 = 96.

3 addition) and "Final" (12 min after DMSO or Compound 3 addition) timepoint and then calculated the ratio of the fluorescence values at the Final versus Initial timepoints along the length of the spindle (Figure 7B). To quantify the magnitude of changes in KIF18A localization over the 12-min time course, the area under the curve for each ratio plot was also determined (Figure 7C). These analyses showed loss of GFP-KIF18A from the middle of the spindle and accumulation at the poles in Compound 3-treated cells, whereas DMSO-treated cells did not exhibit these changes (Figures 7B, C). Combined, the fixed- and live-cell imaging data demonstrate that chemical inhibition of KIF18A with Compound 3 treatment leads to relocalization of the motor from microtubule plus-ends to spindle poles in diploid and chromosomally unstable cell lines, similar to the localization defects observed for KIF18A-S284 mutants.

KIF18A inhibitors cause mitotic arrest and reduced proliferation of chromosomally unstable cells

Given that KIF18A inhibitor treatment mimics the chromosome alignment and spindle length phenotypes observed following KIF18A KD, we predicted that inhibition of KIF18A with Compound 3 or Sovilnesib would lead to mitotic arrest in chromosomally unstable cell lines, but not in diploid cells, as previously observed (Fonseca et al., 2019; Cohen-Sharir et al., 2021; Marquis et al., 2021; Quinton et al., 2021). To test this prediction, we measured the mitotic index in diploid RPE1 cells and the chromosomally unstable cell lines MDA-MB-231 and HT-29. In diploid RPE1 cells, KIF18A inhibitor treatment and KIF18A KD did not affect the mitotic index as compared to treatment with DMSO or control KD (Figures 8A, B; Supplementary Figure S4A). In contrast, MDA-MB-231 and HT-29 cells treated with KIF18A inhibitors or KIF18A siRNAs displayed a significant increase in the mitotic index (Figures 8C–F; Supplementary Figures S4B, S4C). Furthermore, MDA-MB-231 and HT-29 cells displayed a significant increase in multipolar spindles following KIF18A inhibitor treatment, but RPE1 cells did not (Figures 8G, H; Supplementary Figures S4D–S4F). Of note, the HT-29 cells treated with KIF18A inhibitors resulted in a higher percentage of multipolar spindles than of bipolar spindles (Figure 8H; Supplementary Figure S4F). These results suggest that both chemical inhibition of KIF18A and KIF18A KD result in mitotic arrest and abnormal spindle formation in chromosomally unstable cell lines, but not in diploid cells.

To determine whether the mitotic arrest phenotypes observed after KIF18A inhibitor treatment also lead to a decrease in growth, we measured the proliferation of diploid RPE1 and chromosomally unstable MDA-MB-231 and HT-29 cells in increasing concentrations of Compound 3 or Sovilnesib using a kinetic proliferation assay (Marquis et al., 2021). The proliferation of diploid RPE1 cells was unaffected by increasing concentrations of KIF18A inhibitors, up to 1 µM (Figures 9A–C; Supplementary Figures S5A, S5B). In contrast, the proliferation of MDA-MB-

10.3389/fmolb.2024.1328077

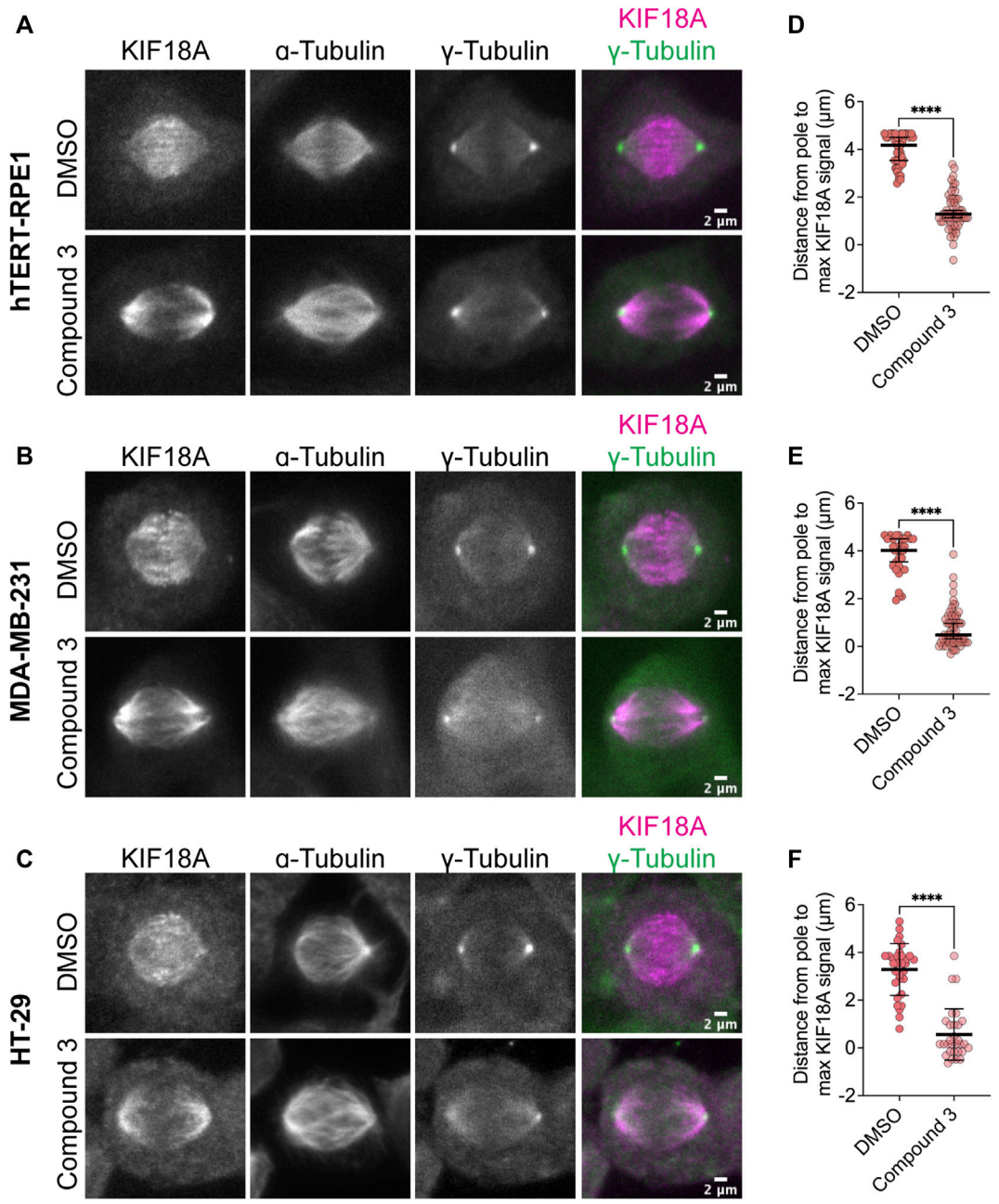

FIGURE 6
Compound 3 disrupts microtubule plus-end localization of KIF18A. **(A–C)** Immunofluorescence images of hTERT-RPE1 **(A)**, MDA-MB-231 **(B)**, and HT-29 **(C)** cells fixed and stained 24 h after DMSO or 250 nM Compound 3 treatment to visualize KIF18A localization. Left to right: KIF18A antibody staining, α-tubulin antibody staining, γ-tubulin antibody staining, merged image of KIF18A (magenta), and γ-tubulin (green) staining. Scale bar: 2 µm. **(D–F)** Plots of distance from the maximum KIF18A signal to the spindle pole derived from the line scan analyses of KIF18A distribution in the indicated cell types. Each dot represents a single cell. Dark bars represent the mean values. Statistical results are shown for a Kruskal–Wallis with Dunn's multiple comparisons test. *p*-value: <0.05 (*), <0.01 (**), <0.001 (***), and <0.0001 (****). The following number of line scans was analyzed for the indicated cell lines and conditions: HT-29 DMSO = 31 line scans, HT-29 Compound 3 = 30 line scans, MDA-MB-231 DMSO = 33 line scans, MDA-MB-231 Compound 3 = 59 line scans, RPE1 DMSO = 42 line scans, and RPE1 Compound 3 = 59 line scans.

231 and HT-29 cells was significantly reduced with increasing concentrations of KIF18A inhibitors (Figures 9D–I; Supplementary Figure S5C–S5F). The increased sensitivity of HT-29 cells to KIF18A inhibitors compared to MDA-MB-231 cells is consistent with our previous findings that the fold decrease in proliferation was inversely correlated with the fold increase in multipolar spindles following KIF18A KD (Marquis et al., 2021). Furthermore, chemical inhibition of KIF18A specifically decreased the proliferation of chromosomally unstable cell lines but did not affect the growth of diploid cells, highlighting the therapeutic potential of KIF18A inhibitors for specifically targeting tumor cells.

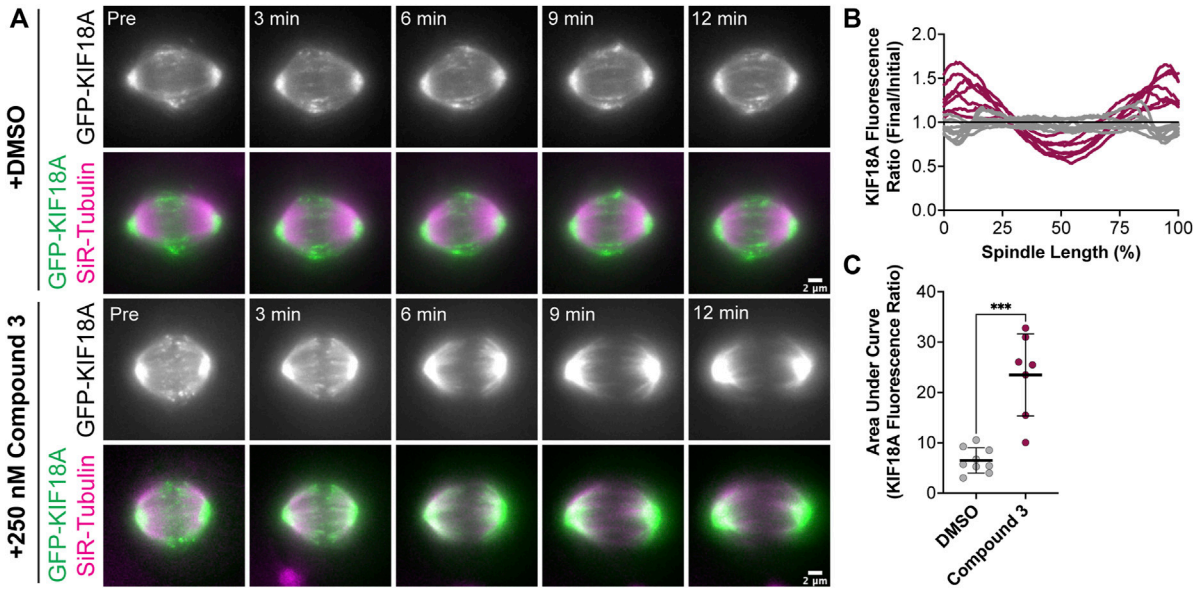

FIGURE 7
Compound 3 leads to rapid relocalization of KIF18A to the poles. **(A)** Time-lapse images of hTERT-RPE1 cells inducibly expressing wild-type GFP-KIF18A after knockdown of endogenous KIF18A. GFP-KIF18A (green) and SiR-tubulin (magenta). Indicated timepoints before ("Pre") and after DMSO or 250 nM. Compound 3 addition. Scale bar: 22 µm. **(B)** Graph of the GFP-KIF18A fluorescence signal (final fluorescence values divided by initial fluorescence values from the region of interest capturing the entire spindle) versus% spindle length (length of individual spindles was normalized on a scale from 0% to 100% for cell-to-cell comparison). Gray lines are DMSO-treated cells, and magenta lines are 250 nM Compound 3-treated cells. Each line represents an individual cell. Data compiled from three experimental replicates. **(C)** Quantification of the area under the curve from the graph in **(B)**. Bars are mean ± standard deviation. Dots represent individual cells from three independent experiments (N = 9 for DMSO, and N = 7 for Compound 3). Statistical analysis results displayed from a Mann–Whitney test. *p*-value style: <0.05 (*), <0.01 (**), <0.001 (***), and <0.0001 (****). n.s. indicates not significant (>0.05).

Discussion

Here, we show that chemical inhibition of KIF18A and mutations that mimic the phosphorylation of the alpha-4 helix lead to alterations in the localization of the motor away from the microtubule plus-ends toward the spindle poles. In addition to resulting in altered localization, both S284 mutations and chemical inhibition resulted in increased chromosome distribution and spindle length. Furthermore, chemical inhibition and S284D mutations resulted in defects in proliferation, an increased mitotic index, and increased multipolarity, specifically in chromosomally unstable cells. These data further support use of KIF18A as a promising target for treatment of CIN tumors.

The similar KIF18A localization pattern caused by chemical inhibition of KIF18A and S284 mutations suggests a possible mechanism of action, whereby the chemical inhibitors induce alterations to the alpha-4 helix of KIF18A. This is consistent with modeling data suggesting that the KIF18A inhibitors tested in this study interact with a hydrophobic pocket of the KIF18A enzymatic domain between the alpha-4 and alpha-6 helices (Tamayo et al., 2022). Localization of KIF18A to spindle poles is different than the effects caused by mutations that are predicted to reduce the interaction of KIF18A with microtubules. In those cases, KIF18A is evenly distributed along microtubules and displays more cytoplasmic localization (Stumpff et al., 2008; Kim et al., 2014; Czechanski et al., 2015). Thus, we hypothesize that S284 mutations and the KIF18A inhibitors tested here may stabilize KIF18A in a conformation that is tightly bound to microtubules. This model is consistent with data indicating that compounds in this chemical series are more effective inhibitors of KIF18A ATPase activity in the presence of microtubules (Tamayo et al., 2022). In this case, the localization of KIF18A protein to spindle poles is explained by the microtubule flux within the spindle, where microtubule-associated KIF18A travels toward the minus-ends of microtubules as they are depolymerized (Mitchison, 1989; Kwok and Kapoor, 2007). Consistent with this idea, a gap in the KIF18A-GFP protein can be seen to expand from the center of the spindle toward the poles from 3 to 12 min after inhibitor treatment (Figure 7A). Thus, trapping KIF18A in a microtubule-bound state may be an effective inhibition strategy for specifically reducing the proliferation of CIN tumor cells.

KIF18A is also required to maintain spindle bipolarity in CIN cells, which subsequently influences their dependence on KIF18A for proliferation (Marquis et al., 2021). In this study, we show that both chemical inhibition of KIF18A and S284D mutations result in aberrant KIF18A localization to spindle poles and subsequent loss of spindle bipolarity. Interestingly, the S284A mutation does not have as pronounced of a localization defect and does not increase the percentage of multipolar mitotic spindles. This lack of increase in multipolarity is correlated with a proliferation rate that more closely mimics that of cells expressing wild-type KIF18A, suggesting that the S284A mutant retains enough function to support mitotic progression. These data suggest KIF18A's roles in maintaining spindle polarity and promoting progression through mitosis as being critical for CIN cell proliferation, consistent with previous

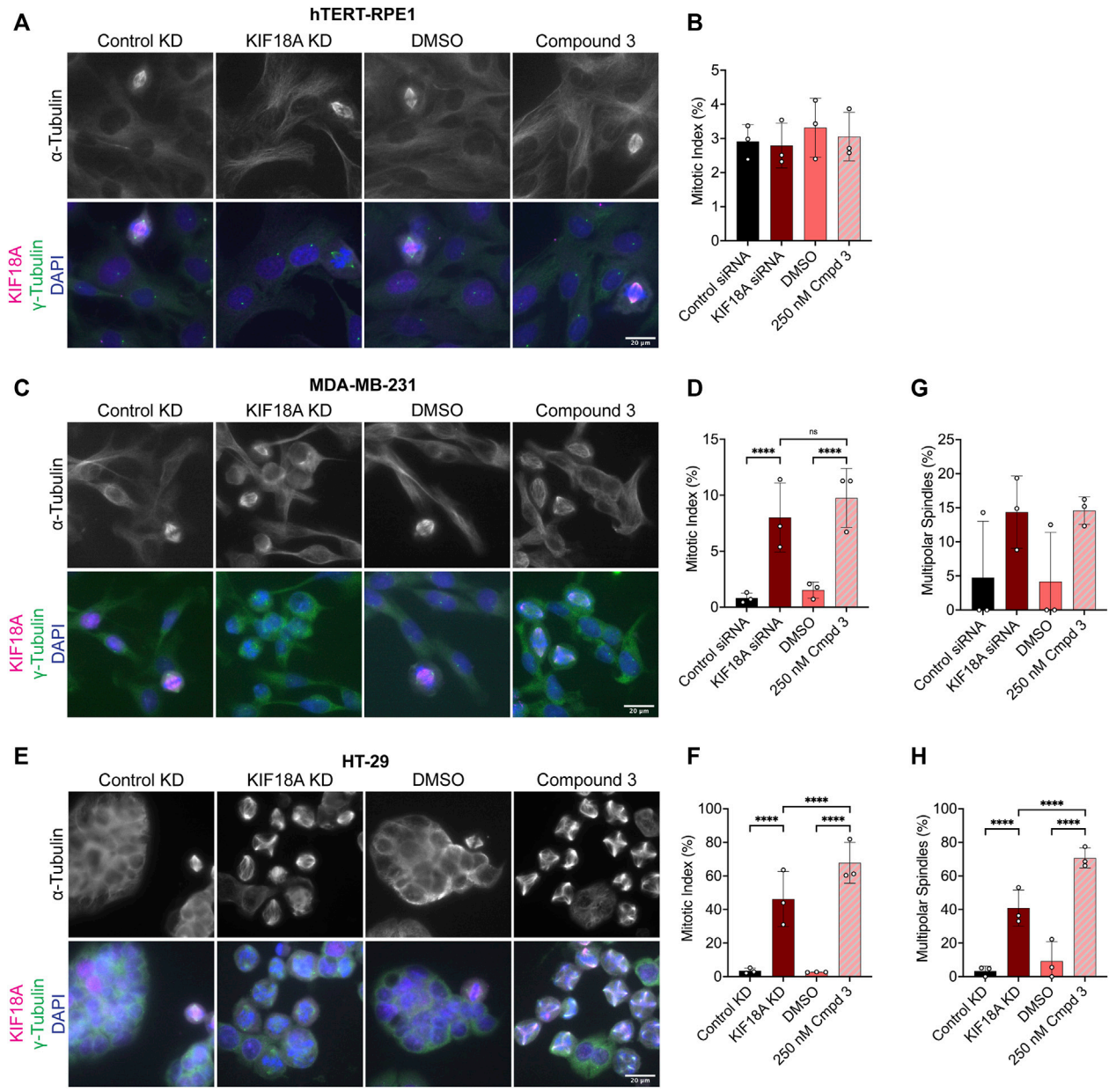

FIGURE 8
Compound 3 treatment leads to mitotic arrest and multipolar spindles in chromosomally unstable breast and colorectal cancer cells. **(A)** Immunofluorescence images of hTERT-RPE1 cells fixed and stained 24 h after indicated treatments. Scale bar: 20 μm. Top: α-tubulin only. Bottom: merged image of γ-tubulin (green), KIF18A (magenta), and DAPI/DNA (blue). **(B)** Quantification of the mitotic index (% of total cells in mitosis) in hTERT-RPE1 cells 24 h after indicated treatments. Bars are mean ± standard deviation. Each dot indicates an experimental replicate. **(C)** Immunofluorescence images of MDA-MB-231 cells fixed and stained 24 h after indicated treatments. Scale bar: 20 μm. Top: α-tubulin only. Bottom: merged image of γ-tubulin (green), KIF18A (magenta), and DAPI/DNA (blue). **(D)** Quantification of the mitotic index (% of total cells in mitosis) in MDA-MB-231 cells 24 h after indicated treatments. Bars are mean ± standard deviation. Each dot indicates an experimental replicate. **(E)** Immunofluorescence images of HT-29 cells fixed and stained 24 h after indicated treatments. Scale bar: 20 μm. Top: α-tubulin only. Bottom: merged image of γ-tubulin (green), KIF18A (magenta), and DAPI/DNA (blue). **(F)** Quantification of the mitotic index (% of total cells in mitosis) in HT-29 cells 24 h after indicated treatments. Bars are mean ± standard deviation. Each dot indicates an experimental replicate. **(G–H)** Quantification of multipolar spindles (% of total spindles) in MDA-MB-231 cells **(G)** and HT-29 cells **(H)** Twenty-four hours after indicated treatments. Bars are mean ± standard deviation. Each dot indicates an experimental replicate. The following total cell numbers was analyzed for each condition and cell line: HT-29: Control siRNA = 2257, KIF18A siRNA = 1319, DMSO = 2014, Compound 3 = 935 cells; MDA-MB-231: Control siRNA = 2298, KIF18A siRNA = 1928, DMSO = 2468, Compound 3 = 2115; RPE1: Control siRNA = 871, KIF18A siRNA = 940, DMSO = 1052, Compound 3 = 1049; HeLa Kyoto Control siRNA = 1558, siRNA = 1402, GFP = 997, GFP-KIF18A WT = 2136, GFP-S284A = 1364, and GFP-S284D = 1574. Data were compared using a chi-squared test. *p*-value style: <0.05 (*), <0.01 (**), <0.001 (***), and <0.0001 (****). n.s. indicates not significant (>0.05), and if no significance is indicated, the result was not significant (>0.05).

observations (Cohen-Sharir et al., 2021; Marquis et al., 2021; Quinton et al., 2021). On the other hand, reduced chromosome alignment and longer spindles in the S284A mutant-expressing cells appear to be tolerable defects that do not result in an immediate reduction in proliferation. Similarly, diploid somatic cells can continue proliferating in the absence of KIF18A activity, despite the

10.3389/fmolb.2024.1328077

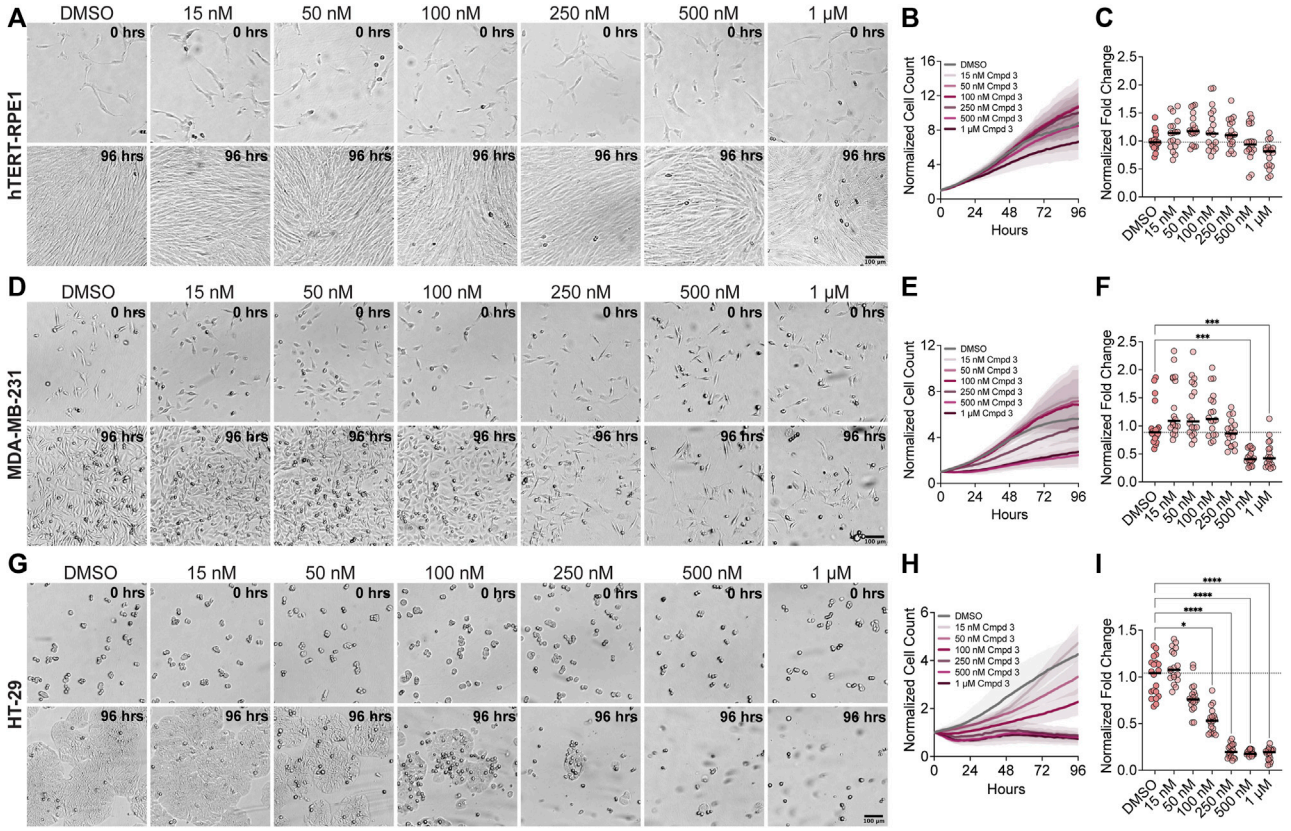

FIGURE 9
Compound 3 reduces the proliferation of chromosomally unstable cells in a dose-dependent manner. **(A)** Brightfield images of hTERT-RPE1 cells from time-lapse proliferation assays with the indicated concentrations of Compound 3. Scale bar: 100 μm. (Top) 0 h and (bottom) 96 h. **(B)** Plot of normalized cell count over time for cells treated with the indicated concentrations of Compound 3. Lines indicate mean, and shaded area denotes SD. **(C)** Plot of normalized hTERT-RPE1 cell count (displayed as a % of DMSO control) as a function of Compound 3 concentration. **(D)** Brightfield images of MDA-MB-231 cells from time-lapse proliferation assays with the indicated concentrations of Compound 3. Scale bar: 100 μm. (Top) 0 h and (bottom) 96 h. **(E)** Plot of normalized cell count over time for MDA-MB-231 cells treated with the indicated concentrations of Compound 3. Lines indicate mean, and the shaded area denotes SD. **(F)** Plot of normalized MDA-MB-231 cell count (displayed as a % of DMSO control) as a function of Compound 3 concentration. **(G)** Brightfield images of HT-29 cells from time-lapse proliferation assays with the indicated concentrations of Compound 3. Scale bar: 100 μm. (Top) 0 h and (bottom) 96 h. **(H)** Plot of normalized cell count over time for HT-29 cells treated with the indicated concentrations of Compound 3. Lines indicate mean, and the shaded area denotes SD. **(I)** Plot of normalized HT-29 cell count (displayed as a % of DMSO control) as a function of Compound 3 concentration. For plots in **(C,F,I)**, each dot indicates an individual well, and bars indicate mean values. Statistical results displayed from a Mann–Whitney test. *p*-value style: <0.05 (*), <0.01 (**), <0.001 (***), and <0.0001 (****). n.s. indicates not significant (>0.05). Data shown on all plots are from three independent experiments.

presence of chromosome alignment defects (Czechanski et al., 2015; Fonseca et al., 2019; Sepaniac et al., 2021). In the case of the S284A mutant, we predict that enough KIF18A activity remains to support mitotic progression, but not chromosome alignment. This potential graded phenotypic response following partial and more complete inhibition of KIF18A is useful to consider when evaluating whether KIF18A inhibitors produce effects that may potentially inhibit CIN tumor proliferation.

This work demonstrates that chemical inhibition of KIF18A closely mimics the differential effects of KIF18A KD in CIN and diploid cells in terms of single-cell phenotypes and suggests the alpha-4 helix as a potential target for effective inhibition. Thus, our results support the idea that KIF18A inhibition may serve as a promising therapeutic treatment for CIN tumor types including breast, colorectal, cervical, and ovarian cancer. Future work will focus on determining how the alpha-4 helix is altered by mutations in S284 or binding to inhibitory compounds.

Materials and methods

Cell culture and transfections

HT-29 and MDA-MB-231 cells were purchased from ATCC. MDA-MB-231 and HT-29 cells were grown in DMEM/F12 medium (Gibco, 11320082) containing 10% FBS (Gibco, 16000044). HeLa Kyoto and RPE1 acceptor cell lines were both generous gifts received from Ryoma Ohi, University of Michigan. HeLa Kyoto and RPE1 cells were cultured at 37°C with 5% CO_2 in MEM-α medium (Gibco, 12561072) containing 10% fetal bovine serum (FBS) (Gibco, 16000044). Acceptor cell lines were maintained in blasticidin (Thermo Fisher Scientific, R21001) until generation of inducible clones, after which cell lines were maintained in puromycin (Thermo Fisher Scientific, A11138-03). For siRNA transfections in a 24-well plate format, MDA-MB-231, HT-29, HeLa Kyoto, and RPE1 cells were treated with 5 pmol siRNA that was preincubated for 5–10 min in Opti-MEM Reduced-

Serum Media (Gibco, 31985062) with a Lipofectamine RNAiMax transfection reagent (Invitrogen, 13778150). KIF18A siRNAs used were a 1:1 mixture of two of the following silencer or silencer select validated siRNAs (5′ to 3' sequence): GCUGGAUUUCAUAAAGUG Gtt (Ambion, AM51334), GCUUGUUCCAGAAUCGAGAtt (Ambion, 4390824), or CGUUAACUGCAGACGUAAAtt (Ambion, 4392420). Control siRNAs used were Ambion Silencer Select Negative Control #2 (Ambion, 4390846), Silencer Negative Control siRNA #2 (Ambion, AM4613), or Silencer Select Negative Control #1 (4390843).

Generation and validation of HeLa Kyoto and RPE1 inducible cell lines

All KIF18A inducible cell lines were generated using previously described methods (Khandelia et al., 2011; Fonseca et al., 2019; Thompson et al., 2022). Briefly, a wild-type KIF18A siRNA and puromycin-resistant plasmid was developed containing loxP sites for recombination-mediated cassette exchange. The loxP-containing plasmid was then transfected into HeLa Kyoto acceptor cells (Sturgill et al., 2016), and cells which had undergone recombination were selected with puromycin. KIF18A wild-type (Czechanski et al., 2015), S284A (generated using mutagenesis), and S284D (generated through mutagenesis) siRNA-resistant fragments and pEM791 vector (Sturgill et al., 2016) were amplified with primers designed for Gibson assembly (New England Biolabs). After confirming the correct sequence of the Gibson assembled plasmid, recombination was achieved by transfecting the acceptor cells with the KIF18A plasmid and recombinase using LTX transfection (Thermo Fisher Scientific). Recombination was initially selected with 1 μg/mL puromycin for 48 h followed by a stricter selection with 2 μg/mL puromycin for 48 h prior to switching back to 1 μg/mL puromycin for HeLa Kyoto cell lines. To generate RPE1 inducible cell lines, recombination was initially selected, with 10 μg/mL puromycin for 72 h followed by a stricter selection with 20 μg/mL puromycin for 72 h prior to switching back to 10 μg/mL puromycin. The resulting KIF18A inducible cell lines were maintained in MEM-α medium (Life Technologies) with 10% FBS (Life Technologies) and 1 μg/mL puromycin (HeLa Kyoto) or 5 μg/mL puromycin (hTERT-RPE1) at 37°C, 5% CO_2.

The resulting inducible cell lines were verified to be correct by extracting genomic DNA (QIAmp DNA Blood Mini Kit, QIAGEN #51106) and sequencing through the S284 mutation site (Eurofins). KIF18A inducible constructs were expressed with 2 μg/mL doxycycline (Thermo Fisher Scientific #BP26531).

Immunofluorescence

Cells were seeded onto 12-mm glass coverslips in 24-well plates and fixed in −20°C methanol (Thermo Fisher Scientific, A412-1) or −20°C methanol with 1% paraformaldehyde (Electron Microscopy Sciences, 15710) for 10 min on ice. The coverslips were then washed three times for 5 min each in Tris-buffered saline (TBS; 150 mM NaCl, 50 mM Tris base, and pH 7.4). The coverslips were blocked for 1 h at room temperature in 20% goat serum in antibody dilution buffer [Abdil: TBS pH 7.4, 1% bovine serum albumin (BSA), 0.1% Triton X-100, and 0.1% sodium azide]. Coverslips were then washed two times in TBS for 5 min each prior to addition of primary antibodies. Primary antibodies were stored at −20 °C, diluted 1:1 in glycerol, and were subsequently diluted in Abdil at indicated concentrations and duration for staining. The coverslips were washed two times in TBS for 5 min each between primary and secondary antibody incubations. The following secondary antibodies conjugated to AlexaFluor 488, 594, or 647 were stored at −20 °C, diluted 1:1 in glycerol, and used at 1:500 dilution in Abdil for 1 h at room temperature (Invitrogen Molecular Probes: A11029, A11013, A11034, A11032, A11037, A11007, A11014, A11076, A21236, A21245, and A21247). The coverslips were washed three times in TBS for 5 min each prior to mounting coverslips with prolong gold anti-fade mounting medium with DAPI (Invitrogen Molecular Probes, P36935).

Microscopy

Fixed- and live-cell images were acquired on a Ti-E inverted microscope (Nikon Instruments) with a Clara cooled charge-coupled device (CCD) or Ti-2E inverted microscope (Andor) with a Prime BSI sCMOS camera (Teledyne Photometrics) with a Spectra-X light engine (Lumencor). Both microscopes are driven by NIS-Element software (Nikon Instruments) and have an environmental chamber at 37°C. Images were acquired with the following Nikon objectives: Plan Apo 40x DIC M N2 0.95 NA, Plan Apo λ 60x 1.42 NA, or Apo TIRF 100x 1.49 NA. Images were processed and analyzed using ImageJ/Fiji (Schindelin et al., 2012; Schneider et al., 2012).

KIF18A expression level quantification in HeLa Kyoto inducible cell lines

After cells had been seeded onto 12-mm glass coverslips in 24-well plates for 24 h, endogenous KIF18A was depleted, as described above, and GFP-KIF18A was induced with 2 μg/mL doxycycline. Twenty-four hours after knockdown and induction, cells were fixed in −20°C methanol (Fisher Scientific, A412-1) for 3 min on ice and stained for rabbit KIF18A 1:100 (Bethyl, A301-080A), guinea pig CENP-C 1:250 (MBL, PD030), and mouse gamma-tubulin 1:500 (Sigma-Aldrich, T5326). All primary antibodies were incubated for 1 h at room temperature with shaking. Twenty random mitotic cells were imaged for each condition per replicate, and the expression level was quantified in ImageJ/Fiji by drawing an ROI around the mitotic spindle and measuring the KIF18A signal within that ROI. The background signal was determined by moving the same ROI to an area with no cells and measuring the GFP signal in that space. The mean background signal for each image was subsequently subtracted from the mean spindle KIF18A signal. All values were then normalized to the mean, background-subtracted KIF18A intensity. Median and 95% confidence interval are reported for three individual biological replicates.

Mitotic index and multipolarity analyses

In a 24-well plate format, MDA-MB-231, HT-29, RPE1, or HeLa Kyoto cells were treated with control siRNA (5 pmol), KIF18A siRNA (5 pmol), DMSO, or Compound 3 (250 nM final concentration). After 24 h, the coverslips were fixed for staining using 1% paraformaldehyde (Electron Microscopy Sciences, 15710) in −20°C methanol. Cells treated with control siRNA, KIF18A siRNA, DMSO, or 250 nM Compound

3 were fixed and stained for mouse anti-γ-tubulin 1:500 (Sigma-Aldrich, T5326), rabbit anti-KIF18A 1:100 (Bethyl, A301-080A), and rat anti-α-tubulin 1:500 (Sigma-Aldrich, MAB 1864). All primary antibodies were incubated for 1 h at room temperature. Twenty random fields of view were acquired for each condition, and the number of mitotic cells and total cells was counted in each field of view. For multipolar counts, the number of poles was determined for each mitotic cell by comparing both the α-tubulin and γ-tubulin channels. Mean and standard deviations are reported from minimum three individual biological replicates for each condition.

Chromosome alignment and spindle length analyses

Cells were seeded into 24-well plates and subsequently treated with control siRNA (5 pmol), KIF18A siRNA (5 pmol), DMSO, Compound 3 (250 nM), or Sovilnesib (250 nM). After 24 h, the coverslips were then fixed for immunofluorescence with 1% paraformaldehyde (Electron Microscopy Sciences, 15710) in −20°C methanol for 10 minutes. Cells were stained with mouse anti-γ-tubulin 1:500 (Sigma-Aldrich, T5326), rabbit anti-KIF18A 1:100 (Bethyl, A301-080A), and human anti-centromere antibody (ACA) 1:250 (Antibodies Inc., 15-235). All primary antibodies were incubated for 1 h at room temperature except for the human ACA antibody, which was incubated at 4°C overnight. As described previously (Stumpff et al., 2012; Kim et al., 2014; Fonseca and Stumpff, 2016), single-focal plane images with both spindle poles in focus were acquired. A boxed region of interest with a fixed height and width defined by the length of the spindle was used to measure the distribution of ACA-labeled kinetochore fluorescence using the plotProfile command in ImageJ/Fiji. The ACA signal intensity was normalized internally to its highest value and plotted as a function of distance along the pole-to-pole axis. These plots were then fitted to a Gaussian curve, and the full-width at half maximum (FWHM) for the Gaussian fit as well as the spindle length are reported for each cell analyzed. Mean and standard deviations are reported from minimum three individual biological replicates for each condition.

For assaying the effects of KIF18A mutants, inducible HeLa Kyoto cell lines were seeded into 24-well plates and subsequently treated with control siRNA (5 pmol) or KIF18A siRNA (5 pmol) and induced with 2 μg/mL doxycycline. After 24 h, the coverslips were then fixed for immunofluorescence with 1% paraformaldehyde (Electron Microscopy Sciences, 15710) in −20°C methanol for 10 min. The cells were then subsequently stained for rabbit GFP (Invitrogen, A11122), rat anti-α-tubulin 1:500 (Sigma-Aldrich, MAB 1864), and mouse anti-γ-tubulin 1:500 (Sigma-Aldrich, T5326) for 1 h at room temperature with shaking. As described previously (Fonseca and Stumpff, 2016; Fonseca et al., 2019), single-focal plane images with both spindle poles in focus were acquired. A boxed region of interest with a fixed height and width defined by the length of the spindle was used to measure the distribution of DAPI-labeled DNA fluorescence using the plotProfile command in ImageJ/Fiji. The DAPI signal intensity was normalized internally to its highest value and plotted as a function of distance along the pole-to-pole axis using a custom macro in MATLAB. These plots were then fitted to a Gaussian curve, and the FWHM for the Gaussian fit as well as the spindle length are reported for each cell analyzed. Mean and standard deviations are reported from minimum three individual biological replicates for each condition.

KIF18A localization analysis in fixed cells

RPE1, MDA-MB-231, and HT-29 cells were treated with either DMSO Compound 3 (250 nM), or Sovilnesib (250 nM) for 24 h and then fixed for immunofluorescence. The following primary antibodies were used at the indicated dilutions: rat anti-α-tubulin 1:500 (Sigma-Aldrich, MAB 1864), rabbit anti-KIF18A 1:100 (Bethyl, A301-080A), and mouse anti-γ-tubulin 1:500 (Sigma-Aldrich, T5326). Single-focal plane images containing the γ-tubulin pole signal were acquired for individual cells. To measure KIF18A localization relative to the spindle pole, a 10-pixel wide line was manually drawn in Fiji from an individual γ-tubulin pole signal toward the center of the spindle. The profile intensities of KIF18A, α-tubulin, and γ-tubulin along that line were measured and recorded using the plotProfile command in ImageJ/Fiji. Each of these profile intensities was normalized internally to its highest value. These normalized line scans were then aligned by peak γ-tubulin intensity and averaged for each pixel distance. The distance from the pole to the maximum KIF18A signal was determined for each aligned line scan. Mean and standard deviations are reported from a minimum of three independent experiments for each construct.

HeLa Kyoto cells for WT, S284A, and S284D cell lines were seeded onto coverslips and knocked down with Lipofectamine RNAiMAX complexed with siRNAs, as described above. The coverslips were simultaneously induced with 2 μg/mL doxycycline. Twenty-four hours after knockdown and induction, cells were fixed in 1% paraformaldehyde in ice-cold methanol for 10 min. The following primary antibodies were used at the indicated dilutions: rat anti-α-tubulin 1:500 (Sigma-Aldrich, MAB 1864), rabbit anti-GFP 1:1000 (Invitrogen, A11122), and mouse anti-γ-tubulin 1:500 (Sigma-Aldrich, T5326). To measure KIF18A localization relative to the spindle pole, a 10-pixel-wide and 6.5-μm-long line was drawn in ImageJ/Fiji from an individual γ-tubulin pole signal toward the center of the spindle. The profile intensities of GFP, α-tubulin, γ-tubulin, and DAPI signal along that line were measured and recorded using the plotProfile command in ImageJ/Fiji. The profile intensities of each were normalized to the highest value. Then, the normalized line scans were aligned to the highest γ-tubulin intensity and averaged for each micrometer distance. Lastly, the distances from the pole to the maximum KIF18A signal were calculated. A Kruskal–Wallis test with Dunn's multiple comparisons test was performed.

Proliferation assays

MDA-MB-231, HT-29, or RPE1 cells were seeded into 24-well plates (Falcon, 353047) and allowed to adhere overnight before adding the indicated concentrations of Compound 3 or Sovilnesib. Approximately 6 h after compound addition, plates were transferred to the Cytation 5 Cell Imaging Multimode Reader (BioTek/Agilent) driven by Gen5 software (BioTek/Agilent). Plates were then imaged every 2 h using a 4x Plan Fluorite 0.13 NA objective (Olympus) until confluency. Gen5 software was used to process images and measure cell counts at each timepoint using high-contrast brightfield imaging. Parameters used to determine the cell count (cell size and light-intensity thresholds) were optimized for each cell line and previously validated (Marquis et al., 2021). To determine the normalized fold-change, the number of cells at the final timepoint was divided by the

number of cells in the first timepoint and normalized to control treatment (DMSO) for each experiment. Data were generated from a minimum of three individual replicates. Proliferation assays for HeLa Kyoto cell lines were performed in a similar manner. HeLa Kyoto cells inducibly expressing GFP, GFP-KIF18A wild type, GFP-KIF18A S284A, or GFP-KIF18A S284D were seeded into 24-well plates (Falcon, 353047) and allowed to adhere overnight. Knockdown of endogenous KIF18A was performed by adding 5 pmol KIF18A siRNA to each well. Simultaneously, the expression of GFP or GFP-KIF18A constructs was induced by addition of 2 μg/mL doxycycline (Thermo Fisher Scientific, BP26531). To determine the normalized fold-change, the number of cells at the final timepoint was divided by the number of cells at the first timepoint and normalized to GFP-KIF18A wild-type for each experiment. Data were generated from minimum three individual replicates.

Live imaging of KIF18A localization in RPE1 cells

RPE1 cells inducibly expressing siRNA-resistant GFP-KIF18A were seeded into glass-bottom 24-well dishes (Cellvis, P24-1.5h-N). Cells were treated with 2 μg/mL doxycycline (Thermo Fisher Scientific, BP26531) to induce the expression of GFP-KIF18A and 5 pmol KIF18A siRNA to deplete endogenous KIF18A. Approximately 1–1.5 h before imaging, cells were transferred into CO_2-independent media (Gibco, 18045088) supplemented with 10% FBS and containing 100 nM SiR-tubulin (Spirochrome, SC002), SPY595-DNA (1:10,000) (Spirochrome, SC301), 10 μM verapamil (Spirochrome, SCV01), and 20 μM MG-132 (Selleck Chemicals, S2619). Images were acquired at 30-s intervals using a Nikon 60x 1.4 NA objective with 1 μm z-sections for 4–7 μm total (5–8 frames). To quantify changes in KIF18A fluorescence, a rectangular ROI encompassing the spindle was drawn and the KIF18A fluorescence within that ROI was measured and recorded using the plotProfile command in ImageJ. The KIF18A fluorescence profile was measured for a timepoint before DMSO or Compound 3 addition (Initial: −1: 30 min before DMSO or Compound 3 addition) and after DMSO or Compound 3 addition (Final: 12 min after DMSO or Compound 3 addition). Spindle lengths were normalized on a 0%–100% scale to account for differences in spindle lengths between cells. The ratio of Final to Initial KIF18A fluorescence was determined by dividing the KIF18A fluorescence values from the final timepoint by the initial timepoint for each individual cell. This ratio was then plotted as a function of % spindle length for each individual cell. To quantify the magnitude of the differences between the Final and Initial KIF18A fluorescence curves, the "Area under the Curve" calculation in GraphPad Prism was used.

Microtubule-stimulated ATPase assay

KIF18A motor activity was measured using an ADP-Glo luminescence assay (Promega, V9101). Pig microtubules (60 μg/mL, cytoskeleton, MT002) and ATP (25 μM) were incubated with a 4-fold serially diluted test compound or DMSO in reaction buffer (15 mM Tris, pH 7.5, 10 mM $MgCl_2$, 0.01% Tween 20, 1% DMSO, and 1 μM paclitaxel) at RT. Human KIF18A (1–417) protein (2.5 nM) was added to initiate the enzymatic reaction, the reaction mixture was incubated at RT for 120 min, and ADP-Glo reagents were added according to the manufacturer's protocol. The luminescence intensity was measured using an EnVision plate reader (PerkinElmer). Percent inhibition for compounds = 100*(positive control signal—sample signal)/(positive control signal–negative control signal), curve fitting, and IC_{50} values were determined by a 4-parameter nonlinear regression equation (variable slope) using GraphPad Prism 8.0 (GraphPad Software).

Data availability statement

The raw data supporting the conclusion of this article will be made available by the authors, without undue reservation.

Ethics statement

Ethical approval was not required for the studies on humans in accordance with the local legislation and institutional requirements because only commercially available established cell lines were used.

Author contributions

KS: conceptualization, data curation, formal analysis, investigation, writing–original draft, and writing–review and editing. KQ: conceptualization, data curation, formal analysis, investigation, writing–original draft, and writing–review and editing. KF: data curation, formal analysis, investigation, writing–original draft, and writing–review and editing. OB: formal analysis, investigation, writing–original draft, and writing–review and editing. WM: formal analysis, investigation, and writing–review and editing. WL: formal analysis, investigation, and writing–review and editing. XG: formal analysis, investigation, supervision, and writing–review and editing. YX: formal analysis, investigation, and writing–review and editing. FA: conceptualization, funding acquisition, supervision, and writing–review and editing. JJ: conceptualization, data curation, supervision, and writing–review and editing. JS: conceptualization, funding acquisition, supervision, writing–original draft, and writing–review and editing.

Funding

The author(s) declare that financial support was received for the research, authorship, and/or publication of this article. This work was supported by NIH R01GM130556 and NIH R35 GM144133 to JS, an NSF GRF 1842491 to KQ, and a University of Vermont Summer Undergraduate Research Fellowship to OB.

Conflict of interest

Authors WM, WL, XG, YX, FA, and JJ are employed by Apeiron Therapeutics.

The remaining authors declare that the research was conducted in the absence of any commercial or financial relationships that could be construed as a potential conflict of interest.

Publisher's note

All claims expressed in this article are solely those of the authors and do not necessarily represent those of their affiliated organizations, or those of the publisher, the editors, and the reviewers. Any product that may be evaluated in this article, or claim that may be made by its manufacturer, is not guaranteed or endorsed by the publisher.

Supplementary material

The Supplementary Material for this article can be found online at: https://www.frontiersin.org/articles/10.3389/fmolb.2024.1328077/full#supplementary-material

References

Atherton, J., Hummel, J. J., Olieric, N., Locke, J., Peña, A., Rosenfeld, S. S., et al. (2020). The mechanism of kinesin inhibition by kinesin binding protein. *Elife* 9, e61481. doi:10.7554/eLife.61481

Bach, D.-H., Zhang, W., and Sood, A. K. (2019). Chromosomal instability in tumor initiation and development. *Cancer Res.* 79, 3995–4002. doi:10.1158/0008-5472.CAN-18-3235

Cohen-Sharir, Y., McFarland, J. M., Abdusamad, M., Marquis, C., Bernhard, S. V., Kazachkova, M., et al. (2021). Aneuploidy renders cancer cells vulnerable to mitotic checkpoint inhibition. *Nature* 590, 486–491. doi:10.1038/s41586-020-03114-6

Czechanski, A., Kim, H., Byers, C., Greenstein, I., Stumpff, J., and Reinholdt, L. G. (2015). Kif18a is specifically required for mitotic progression during germ line development. *Dev. Biol.* 402, 253–262. doi:10.1016/j.ydbio.2015.03.011

du, Y., English, C. A., and ohi, R. (2010). The kinesin-8 Kif18A dampens microtubule plus-end dynamics. *Curr. Biol.* 20, 374–380. doi:10.1016/j.cub.2009.12.049

Ertych, N., Stolz, A., Stenzinger, A., Weichert, W., Kaulfuß, S., Burfeind, P., et al. (2014). Increased microtubule assembly rates influence chromosomal instability in colorectal cancer cells. *Nat. Cell Biol.* 16, 779–791. doi:10.1038/ncb2994

Fonseca, C., and Stumpff, J. (2016). *The mitotic spindle, methods and protocols*. New York: Springer, 253–262.

Fonseca, C. L., Malaby, H. L. H., Sepaniac, L. A., Martin, W., Byers, C., Czechanski, A., et al. (2019). Mitotic chromosome alignment ensures mitotic fidelity by promoting interchromosomal compaction during anaphase. *J. Cell Biol.* 218, 1148–1163. doi:10.1083/jcb.201807228

Gordon, D. J., Resio, B., and Pellman, D. (2012). Causes and consequences of aneuploidy in cancer. *Nat. Rev. Genet.* 13, 189–203. doi:10.1038/nrg3123

Hirokawa, N., Nitta, R., and Okada, Y. (2009). The mechanisms of kinesin motor motility: lessons from the monomeric motor KIF1A. *Nat. Rev. Mol. Cell Biol.* 10, 877–884. doi:10.1038/nrm2807

Jordan, M. A., and Wilson, L. (2004). Microtubules as a target for anticancer drugs. *Nat. Rev. Cancer* 4, 253–265. doi:10.1038/nrc1317

Khandelia, P., Yap, K., and Makeyev, E. V. (2011). Streamlined platform for short hairpin RNA interference and transgenesis in cultured mammalian cells. *Proc. Natl. Acad. Sci.* 108, 12799–12804. doi:10.1073/pnas.1103532108

Kim, H., Fonseca, C., and Stumpff, J. (2014). A unique kinesin-8 surface loop provides specificity for chromosome alignment. *Mol. Biol. Cell* 25, 3319–3329. doi:10.1091/mbc.E14-06-1132

Kwok, B. H., and Kapoor, T. M. (2007). Microtubule flux: drivers wanted. *Curr. Opin. Cell Biol.* 19, 36–42. doi:10.1016/j.ceb.2006.12.003

Lengauer, C., Kinzler, K. W., and Vogelstein, B. (1998). Genetic instabilities in human cancers. *Nature* 396, 643–649. doi:10.1038/25292

Malaby, H. L. H., Dumas, M. E., Ohi, R., and Stumpff, J. (2019). Kinesin-binding protein ensures accurate chromosome segregation by buffering KIF18A and KIF15. *J. Cell Biol.* 218, 1218–1234. doi:10.1083/jcb.201806195

Marquis, C., Fonseca, C. L., Queen, K. A., Wood, L., Vandal, S. E., Malaby, H. L. H., et al. (2021). Chromosomally unstable tumor cells specifically require KIF18A for proliferation. *Nat. Commun.* 12, 1213. doi:10.1038/s41467-021-21447-2

Mayr, M. I., Hümmer, S., Bormann, J., Grüner, T., Adio, S., Woehlke, G., et al. (2007). The human kinesin Kif18A is a motile microtubule depolymerase essential for chromosome congression. *Curr. Biol.* 17, 488–498. doi:10.1016/j.cub.2007.02.036

Mertins, P., Yang, F., Liu, T., Mani, D. R., Petyuk, V. A., Gillette, M. A., et al. (2014). Ischemia in tumors induces early and sustained phosphorylation changes in stress kinase pathways but does not affect global protein levels. *Mol. Cell Proteomics* 13, 1690–1704. doi:10.1074/mcp.M113.036392

Mitchison, T. J. (1989). Polewards microtubule flux in the mitotic spindle: evidence from photoactivation of fluorescence. *J. Cell Biol.* 109, 637–652. doi:10.1083/jcb.109.2.637

Quinton, R. J., DiDomizio, A., Vittoria, M. A., Kotýnková, K., Ticas, C. J., Patel, S., et al. (2021). Whole-genome doubling confers unique genetic vulnerabilities on tumour cells. *Nature* 590, 492–497. doi:10.1038/s41586-020-03133-3

Schindelin, J., Arganda-Carreras, I., Frise, E., Kaynig, V., Longair, M., Pietzsch, T., et al. (2012). Fiji: an open-source platform for biological-image analysis. *Nat. Methods* 9, 676–682. doi:10.1038/nmeth.2019

Schneider, C. A., Rasband, W. S., and Eliceiri, K. W. (2012). NIH Image to ImageJ: 25 years of image analysis. *Nat. Methods* 9, 671–675. doi:10.1038/nmeth.2089

Sepaniac, L. A., Martin, W., Dionne, L. A., Stearns, T. M., Reinholdt, L. G., and Stumpff, J. (2021). Micronuclei in Kif18a mutant mice form stable micronuclear envelopes and do not promote tumorigenesis. *J. Cell Biol.* 220, e202101165. doi:10.1083/jcb.202101165

Solon, A. L., Tan, Z., Schutt, K. L., Jepsen, L., Haynes, S. E., Nesvizhskii, A. I., et al. (2021). Kinesin-binding protein remodels the kinesin motor to prevent microtubule binding. *Sci. Adv.* 7, eabj9812. doi:10.1126/sciadv.abj9812

Stumpff, J., Dassow, G., Wagenbach, M., Asbury, C., and Wordeman, L. (2008). The kinesin-8 motor Kif18A suppresses kinetochore movements to control mitotic chromosome alignment. *Dev. Cell* 14, 252–262. doi:10.1016/j.devcel.2007.11.014

Stumpff, J., Wagenbach, M., Franck, A., Asbury, C. L., and Wordeman, L. (2012). Kif18A and chromokinesins confine centromere movements via microtubule growth suppression and spatial control of kinetochore tension. *Dev. Cell* 22, 1017–1029. doi:10.1016/j.devcel.2012.02.013

Sturgill, E. G., Norris, S. R., Guo, Y., and ohi, R. (2016). Kinesin-5 inhibitor resistance is driven by kinesin-12. *J. Cell Biol.* 213, 213–227. doi:10.1083/jcb.201507036

Tamayo, N. A., Bourbeau, M. P., Allen, J. R., Ashton, K. S., Chen, J. J., Kaller, M. R., et al. (2022). Targeting the mitotic kinesin KIF18A in chromosomally unstable cancers: hit optimization toward an *in vivo* chemical probe. *J. Med. Chem.* 65, 4972–4990. doi:10.1021/acs.jmedchem.1c02030

Thompson, A. F., Blackburn, P. R., Arons, N. S., Stevens, S. N., Babovic-Vuksanovic, D., Lian, J. B., et al. (2022). Pathogenic mutations in the chromokinesin KIF22 disrupt anaphase chromosome segregation. *eLife* 11, e78653. doi:10.7554/eLife.78653

Thompson, S. L., Bakhoum, S. F., and Compton, D. A. (2010). Mechanisms of chromosomal instability. *Curr. Biol.* 20, R285–R295. doi:10.1016/j.cub.2010.01.034

Tischer, J., and Gergely, F. (2018). Anti-mitotic therapies in cancer. *J. Cell Biol.* 218, 10–11. doi:10.1083/jcb.201808077

Weaver, B. A. A. (2014). How Taxol/paclitaxel kills cancer cells. *Mol. Biol. Cell* 25, 2677–2681. doi:10.1091/mbc.E14-04-0916

Zasadil, L. M., Andersen, K. A., Yeum, D., Rocque, G. B., Wilke, L. G., Tevaarwerk, A. J., et al. (2014). Cytotoxicity of paclitaxel in breast cancer is due to chromosome missegregation on multipolar spindles. *Sci. Transl. Med.* 6, 229ra43. doi:10.1126/scitranslmed.3007965